Available online at www.sciencedirect.com
SCIENCE DIRECT®
Pergamon
Cement and Concrete Research 34 (2004) 195–206
CEMENT AND CONCRETE RESEARCH

The interface between natural siliceous aggregates and geopolymers

W.K.W. Lee, J.S.J. van Deventer*

Department of Chemical and Biomolecular Engineering, The University of Melbourne, Parkville, Victoria 3010, Australia

Received 11 September 2002; accepted 10 July 2003

Abstract

The reaction products as well as the formation mechanisms of alkali-activated binders, or geopolymers, have been studied intensively. However, the interface between mineral aggregates, such as sand and/or natural rocks, and geopolymers has not been studied. This paper reports the microstructure and the bonding strength (Mode I bending) of the interface between natural siliceous aggregates and fly ash-based geopolymers. It was found that when the activating solution that contained no or little soluble silicates, the compressive strengths of the geopolymeric binders, mortars and concretes were significantly weaker than those activated with high dosages of soluble silicates. The presence of soluble silicates in the initial activating solution was also effective in improving the interfacial bonding strengths between rock aggregates and geopolymeric mortars. No apparent interfacial transition zone (ITZ) could be identified near the aggregates if the systems were free from chloride contamination. Chloride (KCl) was found to decrease the interfacial bonding strength between the aggregates and the binders probably by causing gel crystallisation near the aggregate surfaces, which resulted in debonding.

Keywords: Geopolymer; Interfacial transition zone; Bond strength; Fly ash; Aggregate

1. Introduction

It is well known that alkali activation of aluminosilicates can produce X-ray amorphous aluminosilicate gels, or geopolymers, with excellent mechanical as well as chemical properties [1–4]. The structural backbone of these aluminosilicate (geopolymeric) gels has historically been depicted as consisting of a three-dimensional framework of SiO_4 and AlO_4 tetrahedra interlinked by shared O atoms. The negatively charged and tetrahedrally coordinated Al(III) atoms inside the network are charge-balanced by alkali metal cations such as Na, K and Ca [1–4]. These gels can be used to bind aggregates, such as sand or natural rocks, to produce mortars and concretes. In other words, geopolymers are inorganic binders that function as the better-known Portland cement.

In ordinary Portland cement (OPC) concrete, the interface between mineral aggregates and cement binder is often described as the interfacial transition zone (ITZ) [5,6]. When compared to the bulk cement phase, the ITZ typically consists of a higher concentration of portlandite crystal (CH) as well as a lower concentration of calcium silicate hydrate (CSH)—the major binding phase within a hydrated Portland cement system [5–11]. Furthermore, the higher porosity of the ITZ [12,13] is significantly higher than that of the bulk cement paste [12,13]. Hence, the ITZ is generally perceived as the weakest region within a mortar and/or concrete structure [14–16]. The high porosity of the ITZ also allows easier penetration of harmful species such as chloride into the concrete structure [17]. For these reasons, much research has been conducted with the aim to improve the chemical nature and microstructure of the ITZ, which will also benefit the mechanical performance and durability of Portland cement mortars and concretes.

Over the last decade, much research has been conducted on the chemical, mechanical and microstructural aspects of geopolymers [1–4]. However, little attention has been paid to the interactions between aggregates and geopolymeric binders. This presents an obstacle to the use of geopolymers

* Corresponding author. Tel.: +61-3-83446619; fax: +61-3-83447707.
E-mail address: jannie@unimelb.edu.au (J.S.J. van Deventer).

0008-8846/$ – see front matter © 2003 Elsevier Ltd. All rights reserved.
doi:10.1016/S0008-8846(03)00250-3

as concrete binders. The current work will therefore investigate the microstructural characteristics and the mechanical performance of the interfaces in geopolymeric concrete systems.

2. Experimental methods

2.1. Materials

Gladstone fly ash (Class F, according to ASTM definitions) was obtained from Queensland Cement Limited, Australia. Kaolin (HR1 grade) was obtained from Commercial Minerals, Sydney, Australia. Solids from different batches were bulk mixed prior to their use and the compositions as determined by fusion analysis using a Siemens SRS3000 sequential X-ray fluorescence (XRF) spectrometer are listed in Table 1. The major crystalline constituents of the fly ash, as suggested by the supplier and checked by our XRD analysis, are α-quartz (SiO_2), mullite ($3Al_2O_3 \cdot 2SiO_2$), hematite (Fe_2O_3) and magnetite (Fe_3O_4). The major crystalline contents of the kaolin are kaolinite ($Al_2Si_2O_5(OH)_4$) and α-quartz (SiO_2). The mean particle size (d_{50}) was 14.1 μm for the fly ash and 0.5 μm for the kaolin. Sodium silicate (Vitrosol N(N40), molar ratio SiO_2/Na_2O = Rm = 3.32, $[SiO_2]$ = 6.63 mol/l (M)) was obtained from PQ Australia. Laboratory-grade reagents (NaOH, KOH, KCl and K_2CO_3) were obtained from Ajax Chemicals Australia. Distilled/deionised water was used throughout the investigations.

The basalt rock was obtained from Australian Slate, Melbourne, Australia, which was pale grey in appearance. From X-ray analysis (XRD) and optical microscopy, the rock consisted predominantly of plagioclase feldspar (albite, disordered and anorthite, disordered), potash feldspar (sanidine, disordered), pyroxene (augite) and quartz, with minor quantities of brucite, gibbsite and clay (kaolinite) filling the vesicles.

The siltstone rock was obtained from Doncaster Quarry, Melbourne, Australia. The physical appearance was grey and the mineralogy consisted predominantly of quartz, chlorite (clinochlore), mica (muscovite and illite), clay (kaolinite) and plagioclase feldspar (albite, disordered).

Table 1
The mass compositions of the raw materials

Oxide	Fly ash (wt.%)	Kaolin (wt.%)
SiO_2	50.0	54.5
Al_2O_3	28.0	29.4
Fe_2O_3	12.0	1.4
CaO	3.5	0.2
MgO	1.3	0.2
Na_2O	0.2	0.1
K_2O	0.7	0.2
TiO_2	1.7	2.8
Other minor oxides	0.6	0.2
Combustibles	2.0	11.0
Total	100.0	100.0

Table 2
The calculated compositions of the geopolymeric products

System[a,b,c]	Activating solution[d]			Aggregate[e]
	$[OH^-]_0$ (M)	$[SiO_2]_0$ (M)	[Salt] (M)	
P-5-0	5	0	–	–
P-5-0.5	5	0.5	–	–
P-5-1	5	1.0	–	–
P-5-2.5	5	2.5	–	–
P-5-2.5-Cl	5	2.5	0.32 (KCl)	–
P-5-2.5-CO₃	5	2.5	0.32 (K_2CO_3)	–
P-10-0	10	0	–	–
P-10-0.5	10	0.5	–	–
P-10-1	10	1.0	–	–
P-10-2.5	10	2.5	–	–
P-10-2.5-Cl	10	2.5	0.32 (KCl)	–
P-10-2.5-CO₃	10	2.5	0.32 (K_2CO_3)	–
M-5-0	5	0	–	T
M-5-0.5	5	0.5	–	T
M-5-1	5	1.0	–	T
M-5-2.5	5	2.5	–	T
M-5-2.5-Cl	5	2.5	0.32 (KCl)	T
M-5-2.5-CO₃	5	2.5	0.32 (K_2CO_3)	T
M-10-0	10	0	–	T
M-10-0.5	10	0.5	–	T
M-10-1	10	1.0	–	T
M-10-2.5	10	2.5	–	T
M-10-2.5-Cl	10	2.5	0.32 (KCl)	T
M-10-2.5-CO₃	10	2.5	0.32 (K_2CO_3)	T
C-5-2.5-B	5	2.5	–	B and T
C-5-2.5-Cl-B	5	2.5	0.32	B and T
C-5-2.5-CO₃-B	5	2.5	0.32	B and T
C-5-2.5-S	5	2.5	–	S and T
C-5-2.5-Cl-S	5	2.5	0.32 (KCl)	S and T
C-5-2.5-CO₃-S	5	2.5	0.32 (K_2CO_3)	S and T
C-10-0-B	10	0	–	B and T
C-10-1-B	10	1.0	–	B and T
C-10-2.5-B	10	2.5	–	B and T
C-10-2.5-Cl-B	10	2.5	0.32 (KCl)	B and T
C-10-2.5-CO₃-B	10	2.5	0.32 (K_2CO_3)	B and T
C-10-0-S	10	0	–	S and T
C-10-1-S	10	1.0	–	S and T
C-10-2.5-S	10	2.5	–	S and T
C-10-2.5-Cl-S	10	2.5	0.32 (KCl)	S and T
C-10-2.5-CO₃-S	10	2.5	0.32 (K_2CO_3)	S and T

[a] *P* = binder/paste; mass solid/solution ratio, excluding aggregates, is 2; mass fly ash/kaolin ratio is 9.
[b] *M* = mortar; mass binder/sand ratio is 0.5.
[c] *C* = concrete; mass mortar/coarse aggregate ratio is 1.
[d] The overall molar Na/K ratio is 0.2 (those from the inorganic salts are excluded).
[e] B = basalt, S = siltstone and T = sand.

2.2. Synthesis

The activating solutions of various compositions were prepared according to Table 2, using the Vitrosol N(N40) sodium silicate solution, NaOH and/or KOH, distilled/deionised water in the appropriate proportions,

with and without inorganic salt (KCl and K_2CO_3) addition. Note that the Na/K ratio of the activating solution as shown in Table 2 does not include those from the added inorganic salts. These activating solutions were allowed to cool to room temperature with stirring before geopolymeric binders, mortars and concretes were synthesised.

Nine parts of fly ash (by weight) were mixed with 1 part (by weight) of kaolin in a rotary mixer overnight. Then, 0.5 parts (by weight) of activating solutions were added to the solid mixture and mixed again for 5 min to produce homogeneous pastes of geopolymeric binders. Geopolymeric mortars were prepared by adding 2 parts (by weight) of sand to 1 part (by weight) of the geopolymeric binders and mixed for another 5 min. One part (by weight) of coarse aggregates of basalt, marble or siltstone was added to 1 part (by weight) of the mortars and mixed for a further 5 min to produce geopolymeric concretes. The compositions of the geopolymeric binders, mortars and concretes are summarised in Table 2. System *P-5-2.5* denotes the geopolymeric binder/paste that was synthesised by activating the fly ash/kaolin mixture with an activating solution of 5 M hydroxyl (OH^-) and 2.5 M soluble silicates. System *M-10-2.5* denotes the geopolymeric mortar that was synthesised by adding the required amount of sand to the binder *P-10-2.5*. System *C-10-2.5-B* is the geopolymeric concrete produced by adding basalt (B) coarse aggregates to mortar *M-10-2.5*. The geopolymeric products were cured at 40 ± 3 °C for 24 h. The samples were then demoulded and cured at 20 ± 3 °C and a relative humidity of $50 \pm 5\%$ under atmospheric pressure until testing.

Samples for interfacial bonding strength determination between rock aggregates and geopolymeric mortars were prepared as shown in Fig. 1. Briefly, a rock slice ($50 \times 25 \times 4.5$ mm) was cut and lightly polished at both sides to minimize variations in surface roughness between different rocks of 4.5 mm height. A plastic strip (25×4.5 mm) was glued to one side of the rock slice to introduce an artificial crack. Freshly prepared mortar layers of the same compositions (10 mm thick) were then "glued" to either side of the rock slice and cured 20 ± 3 °C and a relative humidity of $50 \pm 5\%$ under atmospheric pressure until testing. The resultant sandwich samples were demoulded after 24 h. When the *M-5-2.5* mortar was glued to basalt (B), the resultant sandwich specimen was named B&*M-5-2.5*. Similarly, if siltstone (S) was used, the specimen was named S&*M-5-2.5*. Two days before the interfacial bonding strength was tested, each side of the sandwich samples was glued to a precast mortar beam *M-10-2.5* ($50 \times 25 \times 76.75$ mm) using epoxy resin, as was also practised by Trende and Büyüköztürk [16], so that a sandwich beam of a total length of 178 mm could be tested using the three-point bending set-up as shown in Fig. 1. Note that the experimental set-up in Fig. 1 ensures that the greatest stress is located at the interface between the rock slice and the geopolymeric mortar. Experimental observations also showed that failures indeed occurred at the interface.

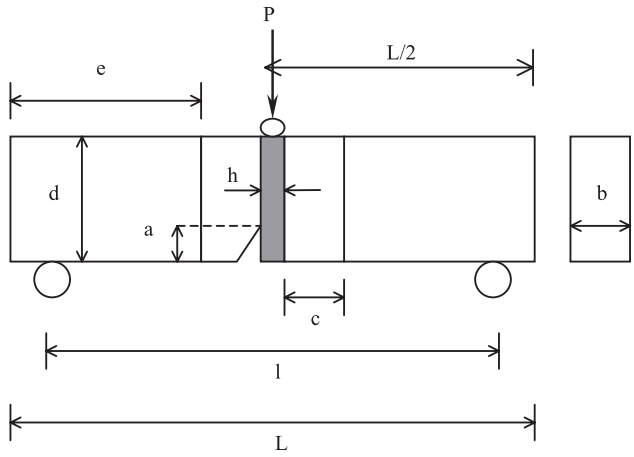

a = 4.5 mm, artificial crack
b = 25 mm, width
c = 10 mm, fresh mortar
d = 50 mm, height
e = 76.75 mm, precast mortar
h = 4.5 mm, thickness, rock slice
l = 100 mm
L = 178 mm, total length
P = load

Fig. 1. The experimental set-up (not to scale) of the three-point bending test on the rock aggregate–mortar sandwich specimens.

2.3. Characterisation/analysis

The compressive strength results were obtained conforming to ASTM C39 on an ELE compression machine using a loading rate of 1 kN/s. The cylindrical sample dimension was 50×100 mm for the binders and the mortars. Larger samples (100×200 mm) were prepared for the concretes. All the values collected were the averages of three separate tests, with a standard deviation of less than 5%.

The three-point bending test on the rock and mortar sandwich specimens was conducted using an Instron 1000 machine at a loading rate of 0.1 mm/min. Failure loads were recorded and then divided by the cross-sectional area of the specimens ($50 \times 25 = 1250$ mm^2) to obtain the interfacial bonding strength, f_i'. All the values collected were the averages of three separate tests. As the sandwich samples were difficult to prepare, the standard deviations of the interfacial bonding strength were rather large between 8.3% and 18.6%.

Scanning electron microscopy (SEM) backscatter electron (BSE) images of the geopolymeric binders and the interface between the aggregates and the binders were obtained using a Philips XL30 SEM coupled with an Oxford Instruments energy dispersive spectrometer (EDS). The sandwich samples were cut cross-sectionally and lightly polished before micrographs were taken. The micrographs of geopolymeric binders were taken on freshly fractured samples.

3. Results

The results of the compressive strength tests on the various geopolymeric binders, mortars and concretes are summarised in Table 3. From Table 3, it was found that when the soluble silicate dosage in the activating solution ($[SiO_2]_0$) was below 2.5 M, the compressive strengths of the resultant salt-free geopolymeric binders and mortars were low regardless of the alkali concentration ($[OH^-]_0$). At $[SiO_2]_0 = 2.5$ M, the product strength was found to increase with increasing alkali concentration in the activating solution. It appears that the product mechanical performance does not only depend on the alkali concentration in the activating solution. Soluble silicates can also play a very important role in determining the product compressive strength.

Table 3
The compressive strengths, f_c', of the geopolymeric products

Specimen	Compressive strength, f_c' (MPa)		
	7 days	28 days	90 days
P-5-0	–[a]	7.0	6.4
P-5-0.5	–[a]	–[a]	–[a]
P-5-1	–[a]	4.7	5.5
P-5-2.5	18.7	36.6	34.1
P-5-2.5-Cl	31.2	25.3	21.2
P-5-2.5-CO_3	22.5	32.8	34.5
P-10-0	–[a]	6.8	8.8
P-10-0.5	7.3	13.7	20.0
P-10-1	5.2	10.8	15.8
P-10-2.5	21.2	41.6	42.4
P-10-2.5-Cl	25.6	40.9	42.8
P-10-2.5-CO_3	27.5	39.8	41.9
M-5-0	–[a]	4.2	4.6
M-5-0.5	–[a]	3.7	3.8
M-5-1	–[a]	6.4	6.7
M-5-2.5	9.8	15.6	19.7
M-5-2.5-Cl	9.5	16.1	20.1
M-5-2.5-CO_3	10.1	15.8	19.6
M-10-0	–[a]	9.1	10.8
M-10-0.5	8.5	15.5	21.3
M-10-1	13.2	26.6	36.6
M-10-2.5	32.2	48.2	60.7
M-10-2.5-Cl	16.1	29.2	36.5
M-10-2.5-CO_3	32.5	47.8	60.2
C-5-2.5-B	9.5	15.8	19.6
C-5-2.5-Cl-B	9.8	15.5	20.1
C-5-2.5-CO_3-B	9.6	16.1	19.5
C-5-2.5-S	9.1	15.9	22.3
C-5-2.5-Cl-S	9.7	15.6	19.8
C-5-2.5-CO_3-S	9.6	16.3	20.3
C-10-0-B	–[b]	7.2	–[b]
C-10-1-B	–[b]	28.3	–[b]
C-10-2.5-B	31.9	49.3	65.9
C-10-2.5-Cl-B	17.8	25.3	33.5
C-10-2.5-CO_3-B	30.5	51.2	66.4
C-10-0-S	–[b]	8.3	–[b]
C-10-1-S	–[b]	28.9	–[b]
C-10-2.5-S	33.4	48.7	63.9
C-10-2.5-Cl-S	18.2	24.8	31.2
C-10-2.5-CO_3-S	29.7	50.7	65.8

[a] Values too low to register.
[b] Not tested.

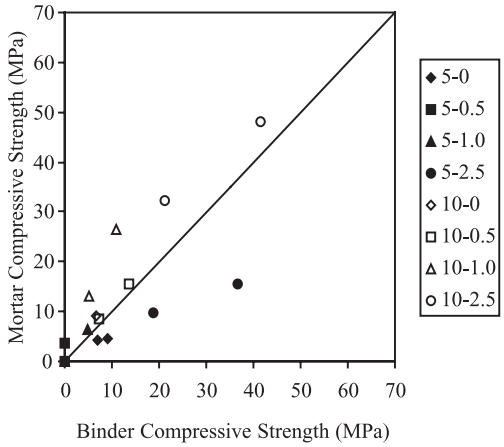

Fig. 2. The compressive strengths of the salt-free binders (*P*) versus the mortars (*M*) for the geopolymeric systems at two alkali concentrations ($[OH^-] = 5$ and 10 M) for 0, 0.5, 1.0 and 2.5 M of soluble silicates added.

Fig. 2 shows that when a 5 M OH^- activating solution was used, addition of sand to a salt-free geopolymeric binder was found to significantly weaken the overall product mechanical performance irrespective of the soluble silicate dosage used. This result is surprising as the compressive strength of the OPC systems is normally increased through the addition of aggregates [18]. On the other hand, if 10 M OH^- activating solutions were used, the geopolymeric mortars were stronger than their binder counterparts. If assuming the differences between the 5 and 10 M OH^- geopolymeric systems were due to the differences in the interfacial bonding capacity between the aggregates and the binders, it is possible that the alkali concentration in the activating solution could determine whether an aluminosilicate gel produced by alkali-activating aluminosilicate solids (fly ash and kaolin) is likely to bind to natural aggregates. This aspect will be further discussed later.

Fig. 3 demonstrates that little difference could be observed between the geopolymeric mortar and the concrete synthesised from the same geopolymeric binder. Again, this does not agree well with the OPC systems where concretes are normally stronger than the mortar counterparts [18]. The chemical and/or physical interactions between the binder and the aggregates are therefore very different in geopolymeric systems as compared to OPC systems. Fig. 3 also shows that the geochemical nature of the coarse aggregates (basalt or siltstone) appeared to have little effect on the geopolymeric concrete compressive strength as shown in Fig. 3. This is consistent with previous experience on the normal OPC concretes. However, in high-performance concretes, which are normally produced by reducing the water/cement ratio through the addition of various water reducers and silica fume, the geochemical properties and surface roughness of the coarse

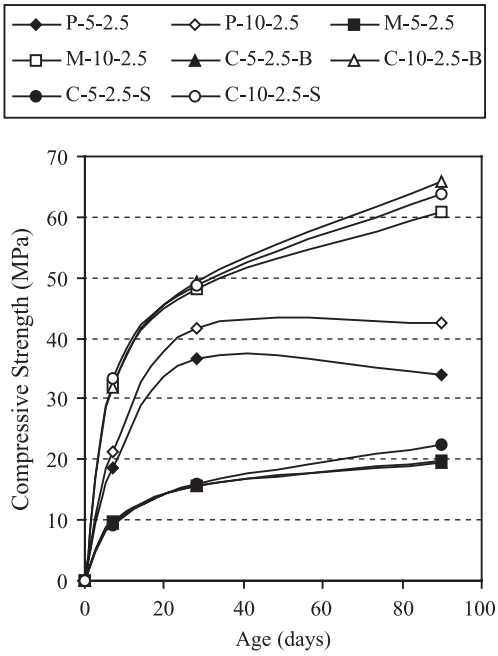

Fig. 3. The time evolution of compressive strengths of the salt-free binders (*P*), the mortars (*M*) and the concretes (*C*) for the geopolymeric systems at two alkali concentrations ([OH^-] = 5 and 10 M).

aggregates are known to affect the overall concrete strength significantly [14–16,18].

From Table 3 and Figs. 2 and 3, it seems that both alkalis and soluble silicates in high concentrations are necessary to synthesise mechanically strong geopolymeric products. Similar conclusions can also be drawn from the three-point bending experiments on the aggregate and salt-free mortar sandwich specimens (see Table 4). When the activating solution was low in alkalis and/or soluble

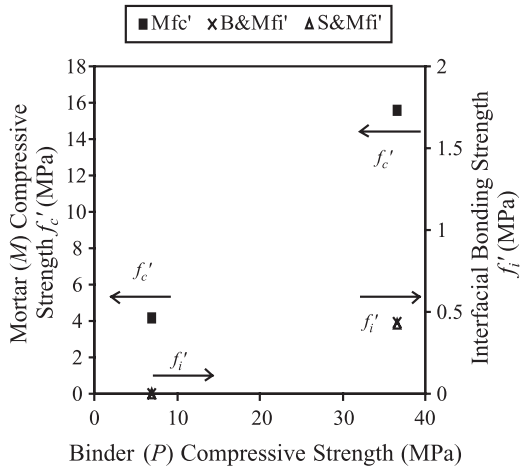

Fig. 4. The binder (*P*) compressive strength versus mortar (*M*) compressive strength and interfacial bonding strength (f_i') for the salt-free geopolymeric systems activated at 5 M OH^- at 28 days.

silicates, the interfacial bonding strengths between the rock slices (basalt and siltstone) and the corresponding salt-free geopolymeric mortars were also low. Furthermore, it seems that the basalt always yielded a slightly stronger interfacial bonding strength than the siltstone. This difference, however, was too small to cause significant differences in the respective concrete compressive strength as shown in Table 3 and Fig. 3.

Trende and Büyüköztürk [16], using similar specimen dimensions as this work but with a Mode I four-point bending set-up, showed that the interfacial bonding strength between a smooth granite aggregate slice and a high-strength cement mortar was 0.503 MPa at 7 days. In that case, the 7_day compressive strength of the mortar was 81.1 MPa and the binder consisted of Type III cement,

Table 4
The interfacial bonding strength, f_i', of the rock and geopolymeric mortar sandwich specimens at 28 days

Specimen	Interfacial bonding strength, f_i' (MPa)
B&*M-5-0*	0[a]
B&*M-5-2.5*	0.44
S&*M-5-0*	0[a]
S&*M-5-2.5*	0.43
B&*M-10-0*	0[a]
B&*M-10-0.5*	0[a]
B&*M-10-1*	0.41
B&*M-10-2.5*	1.27
B&*M-10-2.5-Cl*	0.58
B&*M-10-2.5-CO_3*	1.11
S&*M-10-0*	0[a]
S&*M-10-0.5*	0[a]
S&*M-10-1*	0.41
S&*M-10-2.5*	1.05
S&*M-10-2.5-Cl*	0.57
S&*M-10-2.5-CO_3*	1.06

[a] Values too low to register and are assumed to be 0 MPa.

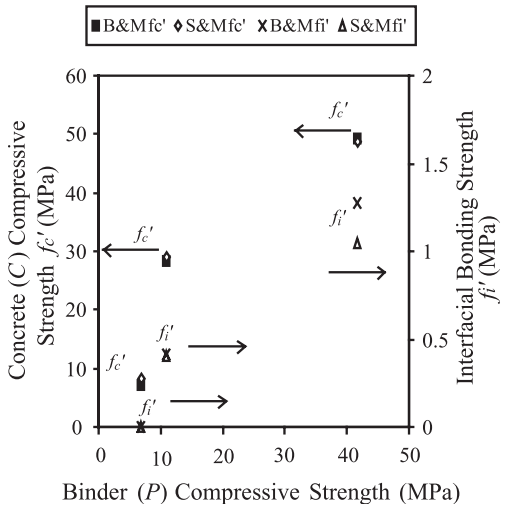

Fig. 5. The binder (*P*) compressive strength versus concrete (*C*) compressive strength and interfacial bonding strength (f_i') for the salt-free geopolymeric systems activated at 10 M OH^- at 28 days.

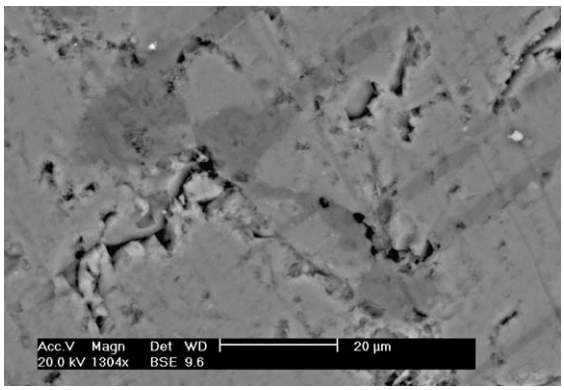

Fig. 6. The SEM image of the mica/clay (F) region of the fresh siltstone (S).

naphthalene sulphonate type superplasticiser and condensed silica fume. This interfacial bonding strength is only ~ 40% of the 28-day interfacial bonding strength of the B&*II-1s0-2.5* sandwich specimen of this work (1.273 MPa, Mode I three-point bending), whose mortar (*II-10-2.5*) compressive strength at 28 days was 48.2 MPa (Table 3). Although direct comparison of the present work with that of Trende and Büyüköztürk [16] should be done with caution due to the different experimental set-up, sample age, rock types, and maybe the aggregate slice surface roughness as well, it nevertheless shows that the geopolymeric binders activated with high concentrations of alkalis and soluble silicates produced very strong bonding with the natural rock aggregates.

A combined examination of the experimental observations described above (Tables 3 and 4 and Figs. 2 and 3) suggests that a strong geopolymeric binder may not necessarily give rise to a strong mortar, concrete and/or aggregate/binder interface. For example, the 28-day compressive strength (Table 3) of binder *P-5-2.5* (36.6 MPa) was significantly higher than that of *P-10-1* (10.8 MPa). The interfacial bonding strengths of the corresponding sandwich specimens S&*M-5-2.5* (0.428 MPa) and S&*M-10-1* (0.405 MPa), however, were similar (Table 4). On the other hand, the 28-day compressive strength of the corresponding mortar *M-5-2.5* (15.6 MPa) was lower than that of *M-10-1* (26.6 MPa). From this result, it appears that no direct relationship could be established between the strengths of geopolymeric binders, mortars, concretes and/or aggregate/binder interface. If, however, the data were plotted separately as shown in Fig. 4 (5 M OH^-) and Fig. 5 (10 M OH^-), a stronger salt-free binder was always associated with a stronger aggregate/binder interface as well as a stronger mortar (Fig. 4), or concrete (Fig. 5).

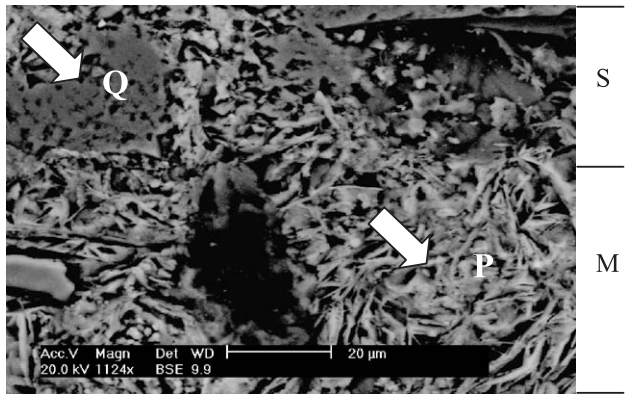

Fig. 8. The SEM image of the sandwich specimen S&*M-10-0* at 28 days. Q = quartz, *P* = binder *P-10-0* and *M* = mortar *M-10-0*. The block arrows indicate where SEM-EDS analyses were taken.

The SEM images taken on the polished siltstone and the polished rock and salt-free mortar sandwich specimens are shown in Figs. 6–13. Fig. 6 shows the fresh siltstone, which serves as a basis of comparison for other experimental conditions. At $[OH^-]_0 = 10$ M and $[SiO_2]_0 = 0$ M, the interface between the siltstone aggregate and the geopolymeric binder *P-10-0* appears to be very porous (Fig. 7). When the soluble silicate dosage was increased from 0 to 2.5 M at the same alkali concentration (Figs. 7–11), it can be seen that the salt-free binder near the interface became

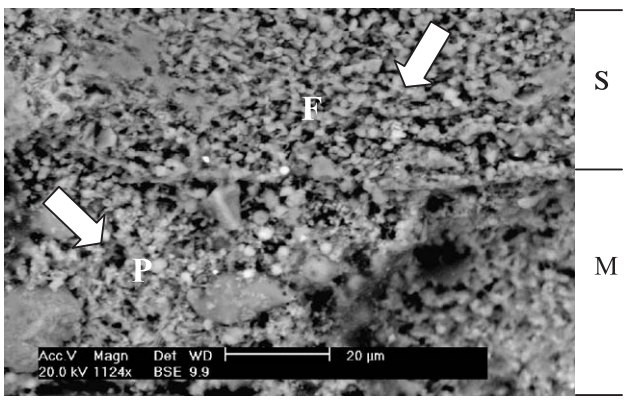

Fig. 7. The SEM image of the sandwich specimen S&*M-10-0* at 28 days. F = mica/clay, *P* = binder *P-10-0* and *M* = mortar *M-10-0*. The block arrows indicate where SEM-EDS analyses were taken.

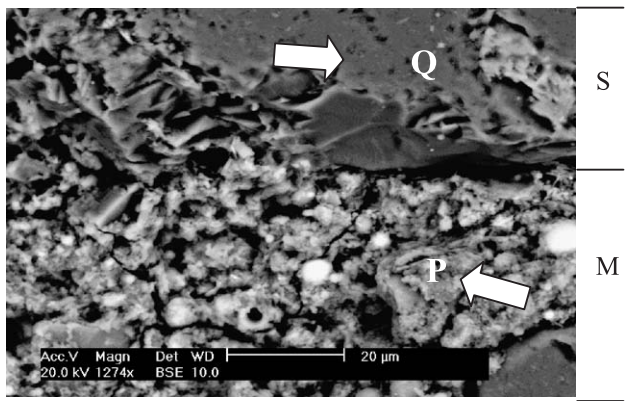

Fig. 9. The SEM image of the sandwich specimen S&*M-10-0.5* at 28 days. Q = quartz, *P* = binder *P-10-0.5* and *M* = mortar *M-10-0.5*. The block arrows indicate where SEM-EDS analyses were taken.

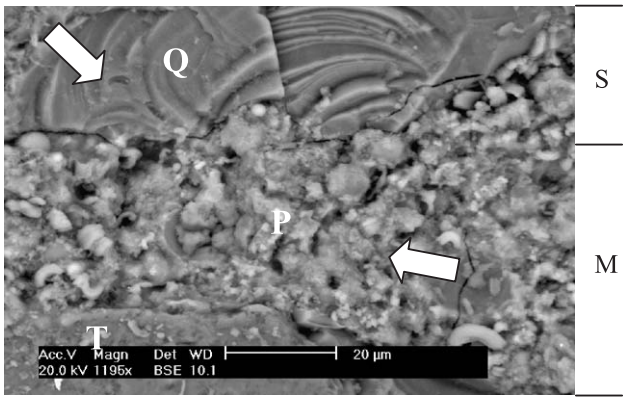

Fig. 10. The SEM image of the sandwich specimen S&*M-10-1* at 28 days. Q = quartz, *P* = binder *P-10-1* and *M* = mortar *M-10-1*. The block arrows indicate where SEM-EDS analyses were taken.

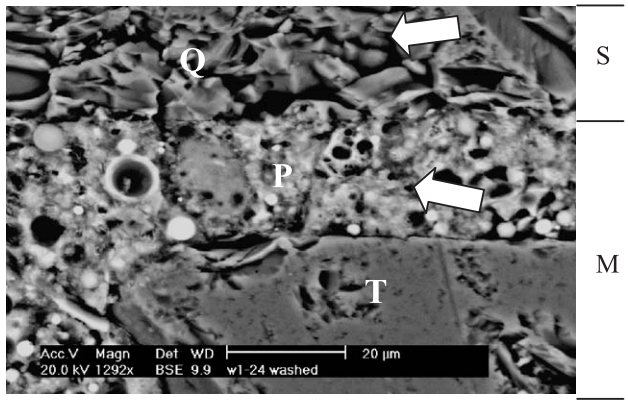

Fig. 12. The SEM image of the sandwich specimen S&*M-5-2.5* at 28 days. Q = quartz, *P* = binder *P-5-2.5* and *M* = mortar *M-5-2.5* and T = sand. The block arrows indicate where SEM-EDS analyses were taken.

denser with increasing soluble silicate dosage. This observation agrees well with the interfacial bonding strengths presented in Table 4. The greater the soluble silicate dosage at a certain alkali concentration, the denser was the aggregate and binder interface and hence the greater was the interfacial bonding strength.

By comparing the images of the sandwich specimens to those of the bulk reference binders (not shown), which were prepared separately under the same experimental conditions as those of the sandwich specimens, it was found that the morphologies of all the interfaces shown in Figs. 7–13 resembled those of the reference binders. A similar conclusion could be drawn from the systems using basalt as the rock slice (not shown). It seems that no clear interface could be identified between the natural aggregates and the salt-free geopolymeric binders, in agreement with other observations on alkali-activated systems [19–21].

Elemental compositions of the various phases in the rock and mortar sandwich specimens were provided by SEM-EDS analyses, as summarised in Table 5. The various rock phases were crudely assigned based on the respective elemental compositions and from the optical microscopy. From Table 5, it is clear that the mica/clay (not differentiable using the current techniques) in Fig. 7 had acquired significant amounts of Na from the alkaline pore solution nearby. (The fresh mica/clay contained only 0.24% of Na and 0.32% of K, whereas the mica/clay in Fig. 8 contained 12.56% of Na and 0.88% of K.) By comparing the SEM images of the sandwich specimen (Fig. 7) with the fresh rock (Fig. 6), together with the SEM-EDS analysis, it is clear that the mica/clay had been corroded by the alkalis in the pore solution nearby if an activating solution was without soluble silicates ($[OH^-]_0 = 10$ M and $[SiO_2]_0 = 0$ M). The depth of the corrosion was approximately 40 μm at the mica/clay region. Alkali corrosion on the rock aggregate, however, was not observed if soluble silicates of high concentration were used as shown in Fig. 13 ($[OH^-]_0 = 10$ M and $[SiO_2]_0 = 2.5$ M). Furthermore, alkali corrosion was found to be phase specific. The region of the rock where quartz was in contact with the alkaline pore solution showed no signs of structural deterioration even when no soluble silicates were used (see Figs. 8–11).

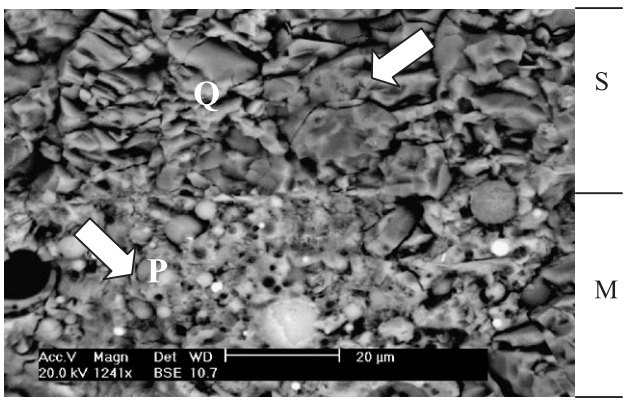

Fig. 11. The SEM image of the sandwich specimen S&*M-10-2.5* at 28 days. Q = quartz, *P* = binder *P-10-2.5*, *M* = mortar *M-10-2.5* and T = sand. The block arrows indicate where SEM-EDS analyses were taken.

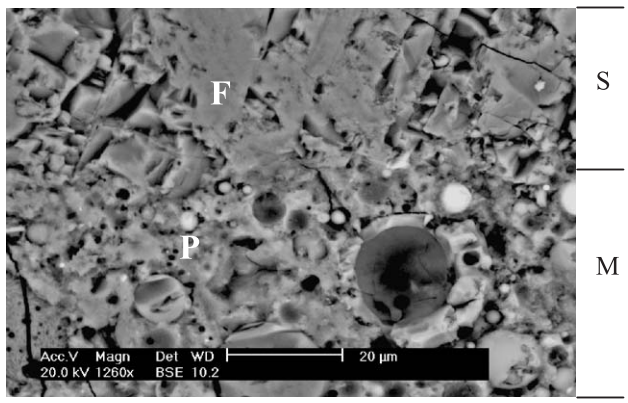

Fig. 13. The SEM image of the sandwich specimen S&*M-10-2.5* at 28 days. F = mica/clay, *P* = binder *P-10-2.5* and *M* = mortar *M-10-2.5*.

Table 5
The SEM-EDS analysis of the siltstone and mortar sandwich specimens at 28 days

Element	Fig. 7, S&*M-10-0*			Fig. 8, S&*M-10-0*			Fig. 9, S&*M-10-0.5*			Fig. 10, S&*M-10-1*			Fig. 11, S&*M-10-2.5*			Fig. 12, S&*M-5-2.5*		
	F[a] (%)		Binder (%)	Q[b] (%)		Binder (%)	Q[b] (%)		Binder (%)	Q[a] (%)		Binder (%)	Q[b] (%)		Binder (%)	Q[b] (%)		Binder (%)
	Before[c]	After		Before[c]	After		Before[c]	After[d]		Before[c]	After		Before[c]	After		Before[c]	After	
O	48.79	46.81	53.91	48.20	48.08	55.33	48.50	–	57.19	48.50	48.02	54.19	48.50	48.06	49.74	48.50	54.17	48.29
Si	36.98	29.45	14.17	50.35	50.60	4.33	50.05	–	5.35	50.05	50.43	10.97	50.05	48.49	19.66	50.05	43.26	18.69
Al	11.05	8.60	5.08	0.00	0.00	2.08	0.00	–	3.22	0.00	0.00	8.00	0.00	0.00	10.59	0.00	0.00	10.90
Fe	0.55	0.63	1.93	0.35	0.45	2.41	0.35	–	2.04	0.35	0.08	2.71	0.35	0.29	1.04	0.35	1.81	2.74
Ca	0.80	0.42	3.90	0.02	0.00	7.77	0.02	–	0.76	0.02	0.17	2.51	0.02	0.11	2.22	0.02	0.00	2.03
Mg	0.71	0.00	0.11	0.00	0.00	0.03	0.00	–	0.00	0.00	0.00	0.04	0.00	0.00	0.11	0.00	0.00	0.10
Na	0.24	12.56	0.18	0.00	0.00	0.07	0.00	–	5.78	0.00	0.06	3.58	0.00	1.63	3.10	0.00	0.00	3.13
K	0.32	0.88	19.34	0.42	0.41	25.72	0.42	–	24.47	0.42	0.47	16.27	0.42	0.73	12.44	0.42	0.18	12.58
Ti	0.08	0.09	0.61	0.00	0.01	0.29	0.00	–	0.50	0.00	0.05	0.60	0.00	0.00	0.00	0.00	0.00	0.41
P	0.30	0.43	0.40	0.66	0.45	0.22	0.66	–	0.21	0.66	0.66	0.30	0.66	0.63	0.66	0.66	0.54	0.30
S	0.14	0.04	0.17	0.00	0.00	1.75	0.00	–	0.48	0.00	0.06	0.26	0.00	0.00	0.23	0.00	0.00	0.70
Cl	0.04	0.09	0.20	0.00	0.00	0.00	0.00	–	0.00	0.00	0.00	0.57	0.00	0.06	0.21	0.00	0.04	0.13
Total	100.00	100.00	100.00	100.00	100.00	100.00	100.00	–	100.00	100.00	100.00	100.00	100.00	100.00	100.00	100.00	100.00	100.00

[a] F = mica/clay (not differentiated).
[b] Q = quartz.
[c] Values are averages of five different analyses on five separate locations. The standard deviation of the mica/clay was 5.3–15.6% and 2.3–3.7% for the quartz depending on the element.
[d] Not tested.

SEM-EDS analysis also showed that little change in the alkali content within the quartz could be identified before and after making contact with the alkaline solution.

Table 3 shows that the addition of inorganic salts (KCl and K_2CO_3) to the activating solutions containing 2.5 M soluble silicates can cause significant differences to the compressive strengths of the binders, the mortars and the concretes. At 5 M OH^-, the chloride was found to accelerate the early strength development of the binder *P-5-2.5-Cl*, reaching the maximum of 31.2 MPa in 7 days. The product then became weaker with time, indicating that the aluminosilicate gel deterioration had initiated between 7 and 28 days. The carbonate, on the other hand, did not adversely affect the product performance. If a solution of 10 M OH^- and 2.5 M soluble silicates was used, addition of both the chloride and the carbonate salts seems to exert no apparent effects on the product compressive strength. This agrees well with the previous investigation by Lee and Van Deventer [22].

From Table 3, aluminosilicate gel deterioration of the system activated with 5 M OH^- and 2.5 M soluble silicates (*P-6-2.5-Cl*) appears to have little effect on the mortar and the concrete compressive strengths at the same degree of chloride contamination (0.32 M). This perhaps is because the mortar (*M-5-2.5*) and the concretes (*C-5-2.5-B* and *C-5-2.5-S*) were already significantly weaker than the binder (*P-5-2.5*) without salt contamination. However, if a solution of 10 M OH^- and 2.5 M soluble silicates was used, it was found that the chloride-contaminated mortar (*M-10-2.5-Cl*) and concretes (*C-10-2.5-Cl-B* and *C-10-2.5-Cl-S*) were significantly weaker than the salt-free (*M-10-2.5*, *C-10-2.5-B* and *C-10-2.5-S*) and the carbonate-contaminated counterparts (*M-10-2.5-CO_3*, *C-10-2.5-CO_3-B* and *C-10-2.5-CO_3-S*). Lee [23] had previously shown that more of the binding phase (aluminosilicate gel) was produced by the 10 M OH^- and 2.5 M soluble silicate activating solution than the 5 M OH^- and 2.5 M soluble silicate counterpart. This is probably why the 10 M OH^- (*P-10-2.5*) activated geopolymeric binder seems to be unaffected by the 0.34 M chloride contamination, whereas the effect was quite noticeable in the 5 M OH^- activated binder (*P-5-2.5*) (see Table 3).

Lee and Van Deventer [22,24] had previously shown that chloride contamination is likely to cause precipitation and crystallisation of the aluminosilicate gels in the geopolymeric binders (gel deterioration). In this work, the SEM micrographs, as shown in Figs. 14–16, reconfirm that, regardless of the alkali concentrations used (OH^- = 5 M and 10 M), potassium-rich aluminosilicates with crystalline

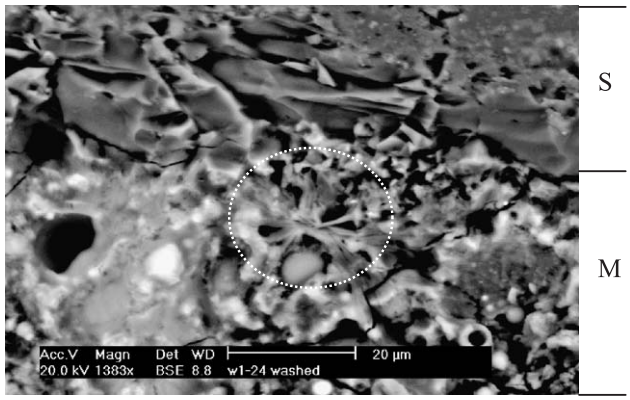

Fig. 14. The SEM image of the sandwich specimen S&*M-5-2.5-Cl* at 28 days.

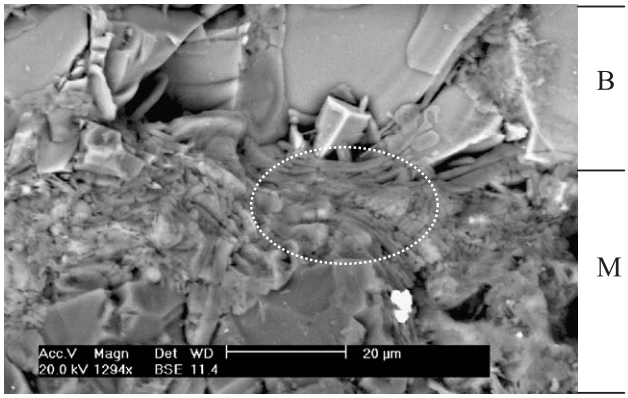

Fig. 15. The SEM image of the sandwich specimen B&*M-10-2.5-Cl* at 28 days.

appearances, whose elemental compositions are presented in Table 6, were indeed present in the chloride-contaminated geopolymeric systems activated with significant soluble silicate dosages. As shown in Figs. 15 and 16 and Table 6, two crystalline phases were present in the chloride-contaminated samples. The crystal morphology and composition were probably determined by the relative proportion of the Si, Al, Na and K of the gel before crystallisation.

The chloride-induced crystals were found to mainly concentrate at the aggregate (basalt, siltstone and sand) surfaces and very few were found in the bulk binders. This aluminosilicate crystallisation at the aggregate surfaces is probably why debonding occurred between the aggregates and the chloride-contaminated mortars. The interfacial bonding strengths between the basalt (0.579 MPa) and the siltstone (0.565 MPa) and *M-10-2.5-Cl* mortar were significantly lower than the salt-free systems (1.273 and 1.048 MPa, respectively) (see Table 4). Consequently, a weak mortar strength (*M-10-2.5-Cl*) as well as weak concrete strengths (*C-10-2.5-Cl-B* and *C-10-2.5-Cl-S*) were observed due to chloride contamination (see Table 3). On the other hand, the carbonate contamination seems to exert no effect on the nature of the aluminosilicate gel formed, nor the interfacial bonding strength between aggregates and geopolymeric binders. Hence, the strengths of the mortar and the concretes were not adversely affected.

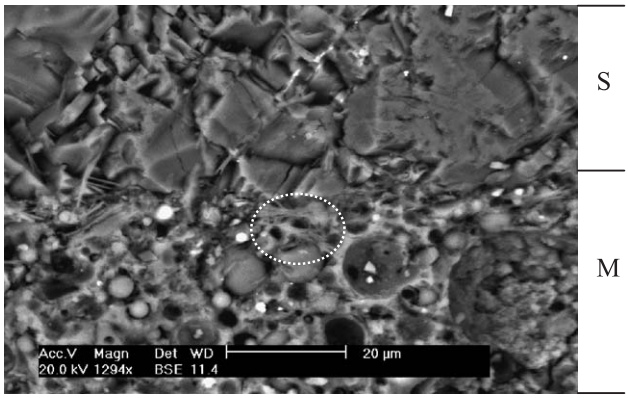

Fig. 16. The SEM image of the sandwich specimen S&*M-10-2.5-Cl* at 28 days.

Table 6
The SEM-EDS analysis of the chloride-induced potassium aluminosilicate crystals from the siltstone and mortar sandwich specimens at 28 days

Element	Elemental composition (%)[a]		
	Fig. 14	Fig. 15	Fig. 16
O	64.05	62.48	66.74
Si	11.61	5.18	11.65
Al	4.06	1.32	4.59
Fe	1.13	2.88	1.04
Ca	1.36	0.20	1.22
Mg	0.31	4.36	0.11
Na	2.16	0.31	1.11
K	13.43	22.41	12.44
Ti	0.00	0.00	− 0.06
P	0.69	0.21	0.66
S	0.30	0.47	0.23
Cl	0.90	0.18	0.21
Total	100.00	100.00	100.00

[a] SEM-EDS was conducted at the white dotted circles as shown in Figs. 14, 15 and 16.

4. Discussion

All the major ITZ models developed for the OPC systems [8,9,25] originate from the fact that at the beginning of the hydration, the region close to the aggregates has on average less cement grains and is instead filled with water. Ions of Ca, Si, Al, Na, K, S and others have to diffuse from the cement grains, or from the aggregate, to this water-rich region so that the formation of the ITZ is possible.

It is now general knowledge that during cement hydration, ions are released from the cement grains to the surrounding solution. How far or how fast an individual ion can travel in the solution depends on its diffusivity as well as the phase equilibrium, which encompasses all the chemical species nearby. In early hydration, the OPC grains are known to release a large amount of Ca into the surrounding solution almost immediately upon contact with water [26]. This in turn increases the solution pH until supersaturation with respect to $Ca(OH)_2$ is reached. The Ca then starts to precipitate out and crystallise as CH in the solution away from the cement grains [27]. The CH acts as a buffer to ensure that the system is always saturated with $Ca(OH)_2$. Although there is evidence that Si can be released into the solution at the same time as Ca [11,28], it is widely observed that Si precipitates out and nucleates at the cement grains as CSH even at the very early stage of hydration before CH crystals can be observed [28]. This is due to the fact that the solubility of Si is limited by the presence of Ca [29]. The CSH then grows outward into the surrounding solution as hydration proceeds [28,30,31]. The pore solution of the OPC systems away from the cement grains therefore contains low concentration of Si while it is being saturated

with $Ca(OH)_2$ [32]. According to Breton et al. [5], this is what accounts for the high CH content of the ITZ. Similarly, CH is often found in the voids and/or (micro)cracks within OPC concretes.

The high CH content of the ITZ is generally believed as one of the reasons why OPC concretes often fail at the aggregate/binder interface. Improving the ITZ properties, therefore, is important in achieving high mechanical performance of concrete structures especially in high-performance concretes. For those that achieved major improvements in increasing the interfacial bonding strength [33,34], the ITZ was reported to exhibit a lower Ca/Si ratio as well as a lower porosity than the normal OPC systems. The CH crystal content was much reduced while the CSH content was increased. According to Kjellsen et al. [33], an ITZ with no measurable or observable difference to the bulk cement phase could be obtained if the water/solid ratio was reduced to 0.25 in conjunction with 10% silica fume replacement. A similar result was reported in high-volume fly ash concretes [35]. In these systems, the "excessive" Ca (those that are not participating directly in the CSH formation) was consumed by the pozzolanic reactions with the silica fume grains (or fly ash) to form more CSH [36–38]. The original voids in the OPC concretes were thus filled with "additional" CSH and consequently a denser ITZ was formed. This implies that a true two-phase system consisting of just the aggregates and the binder could exist if excessive Ca and water were avoided.

In geopolymers, aluminosilicate gel is the major binding phase that provides interparticle bonding and hence the macroscopic strength [1–4]. As the aluminosilicate gel network has the capacity to incorporate calcium [1,29], calcium-substituted aluminosilicate can also exist if there is a calcium source present. It is also suspected that CSH can coexist with (calcium)-aluminosilicate if a high-calcium aluminosilicate solid, such as blast furnace slag, is used [39]. In this work, low calcium-content fly ash (Class F, ASTM definition) and HR1-grade kaolin, which was also low in calcium, were used as the solid raw materials for the geopolymer synthesis. As Ca was incorporated in the aluminosilicate gel network, the pore solution was not saturated with $Ca(OH)_2$. Indeed, no CH crystals could be identified in any of the various geopolymeric products anywhere throughout this investigation.

As shown in Figs. 7 and 8, when no soluble silicate was used, the salt-free geopolymeric binder *P-10-0* was found to consist of two major phases. A region of discrete spherical particles (Fig. 8) of potassium aluminosilicate(s) (see Table 5) was located near the mica/clay region of the siltstone aggregate. Within this region, little interparticle bonding could be observed. On the other hand, elongated, potassium-rich and silicon (and aluminium)-depleted secondary products (Table 5) were found near the quartz region of the siltstone aggregate. The elongated potassium secondary products were also found in the voids away from the aggregate and binder interface-an indication that the system was oversaturated with potassium (hydroxide). These two phases coexisted near the aggregate and binder interface as well as in the bulk. This is probably the reason why the interface of S&*M-10-0* appeared to be very porous. As a result, little interfacial bonding strength (Table 4) was observed between natural aggregates (basalt and siltstone) and *M-10-0* mortar. The high porosity of *P-10-0* could also contribute to the weak compressive strengths observed in *P-10-0*, *M-10-0*, *C-10-0-B* and *C-10-0-S* as shown in Table 3.

Increasing soluble silicate dosage in the activating solution from 0 to 2.5 M was found to be effective in reducing the formation of the elongated potassium secondary products (see Figs. 9–11, 13). In fact, no such compound could be unambiguously identified in the systems activated by the solutions of 0.5, 1 and 2.5 M soluble silicates at 10 M OH^- alkali concentration. The addition of soluble silicates, hence, reduced the oversaturation of potassium (hydroxide) in geopolymeric systems. In effect, this is similar to adding pozzolans (such as silica fume and fly ash) to reduce the CH contents in Portland cement systems as discussed above.

From Figs. 9 and 10, the discrete spherical aluminosilicate particles were found to persist with increasing soluble silicate dosage from 0.5 to 1.0 M, although there were signs that greater interparticle bonding could exist between particles when increasing soluble silicate dosage was used. When 2.5 M of soluble silicates were used at 10 M OH^- alkali concentration, the SEM images (Figs. 11 and 13) suggest that the entire binder was bonded as a whole. No loose particles were identified and the good cohesion even existed between the aggregates and the salt-free binder (Table 4 and Figs. 11 and 13). As a result, improvements were observed in the binder, mortar, concrete and interfacial bonding strengths with increasing soluble silicate dosage at 10 M OH^- (Tables 3 and 4).

From the above, it seems that the interparticle bonding within the salt-free geopolymeric systems was solely provided by the added soluble silicates. This is true if only one alkali concentration is considered. If, however, the results of the systems activated by 10 M OH^- and 2.5 M soluble silicates were compared with those of 5 M OH^- at the same soluble silicate dosage, different conclusions could be reached. From Tables 3 and 4, the binder, the mortar, the concrete as well as the interfacial bonding strengths produced from the 10 M OH^- activating solution were all significantly greater than those of the 5 M OH^- counterparts at the same soluble silicate dosage (2.5 M). If the macroscopic strengths of geopolymeric products are assumed to be largely controlled by the interparticle bonding, either within the binder itself or between the binder and the aggregate surfaces, then the 10 M OH^- activating solution can be understood to provide more of the binding phase than that of the 5 M OH^- solution, as was proved by Lee [23]. As increasing alkali concentration is known to induce greater aluminosilicate dissolution [40], it therefore appears that the strengths of the various geopolymeric products are not only a function of the added soluble silicates. The extent

of dissolution of the aluminosilicate raw materials (and/or the aggregates) is also a major contributor towards the product strengths. This is despite the fact that few morphological differences could be identified between the systems of 5 M OH^- (Fig. 13) and 10 M OH^- (Figs. 11 and 13) at 2.5 M soluble silicate dosage.

When a chloride salt (KCl) was added to the activating solution containing 10 M OH^- and 2.5 M soluble silicates, potassium-rich aluminosilicate crystals were found at the aggregate surfaces as shown in Figs. 15 and 16 and Table 6. Although the chloride-contaminated binder strength at 28 days (*P-10-2.5-Cl*, 40.9 MPa) was close to that of the salt-free binder (*P-10-2.5*, 41.6 MPa), it was apparent that the interfacial bonding strength (Table 4) was significantly decreased due to the chloride-induced gel deterioration. The fact that the chloride-contaminated mortar (*M-10-2.5-Cl*) and concretes (*C-10-2.5-Cl-B* and *C-10-2.5-Cl-S*) were also significantly weaker than the salt-free systems suggests that, within these geopolymeric systems, the interfacial bonding strength may be the critical factor in determining the overall mortar and/or concrete strengths.

5. Conclusion

This work shows that, at high soluble silicate dosage, the interface between siliceous aggregates and geopolymeric gels in salt-free geopolymeric mortars and concretes is not obvious. The interface was found to morphologically resemble that of the bulk binder. It was also found that the effects of soluble silicate addition were twofold. At first, soluble silicates were effective in reducing alkali saturation in the concrete pore solution even when highly alkali-concentrated activating solution was used. Secondly, they promoted greater interparticle bonding within the geopolymeric binders, as well as to the aggregate surfaces. As a result, denser binders as well as stronger aggregate/binder interfaces were formed with increasing soluble silicate dosage. This then led to stronger geopolymeric products including binders, mortars and concretes. If the interfacial bonding between aggregates and geopolymeric binder activated with high dosages of soluble silicates was interrupted by, for example, KCl-induced gel crystallisation, the overall mortar and concrete strengths were shown to significantly weaken as compared to the salt-free systems. Therefore, the interfacial bonding between aggregates and geopolymeric binders is the critical factor in determining the mechanical strengths of the geopolymeric mortars and concretes.

Acknowledgements

The financial support received from Defor and the Particulate Fluids Processing Centre, a Special Research Centre of the Australian Research Council, is greatly appreciated.

References

[1] J. Davidovits, Geopolymers: inorganic polymeric new materials, J. Mater. Eng. 16 (1994) 91–139.
[2] J.G.S. Van Jaarsveld, J.S.J. Van Deventer, The potential use of geopolymeric materials to immobilize toxic metals: Part I. Theory and applications, Miner. Eng. 10 (1997) 659–669.
[3] A. Palomo, M.W. Grutzeck, M.T. Blanco, Alkali-activated fly ashes—a cement for the future, Cem. Concr. Res. 29 (1999) 1323–1329.
[4] D.M. Roy, Alkali-activated cements: opportunities and challenges, Cem. Concr. Res. 29 (1999) 249–254.
[5] D. Breton, A. Carles-Gibergues, G. Ballivy, J. Grandet, Contributions to the formation mechanism of the transition zone between rock–cement paste, Cem. Concr. Res. 23 (1993) 335–346.
[6] M.R. de Rooij, Syneresis in Cement Paste Systems, PhD Thesis, Delft University Press, The Netherlands, 2000.
[7] L. Struble, J. Skalny, S. Mindess, A review of the cement–aggregate bond, Cem. Concr. Res. 10 (1980) 277–286.
[8] R. Zimbelmann, A contribution to the problem of cement–aggregate bond, Cem. Concr. Res. 15 (1985) 801–808.
[9] P.J.M. Monteiro, P.K. Mehta, Improvement of the aggregate–cement paste transition zone by grain refinement of hydration products, 8th International Congress on the Chemistry of Cement, vol. III, 1986, pp. 433–437, Rio de Janeiro.
[10] C.Z. Yuan, I. Odler, The interfacial zone between marble and tricalcium silicate paste, Cem. Concr. Res. 17 (1987) 784–792.
[11] M. Zhang, O.E. Gjorv, Microstructure of the interfacial zone between lightweight aggregate and cement paste, Cem. Concr. Res. 20 (1990) 610–618.
[12] K.L. Scrivener, A. Bentur, P.L. Pratt, Quantitative characterization of the transition zone in high-strength concretes, Adv. Cem. Res. 1 (1988) 230–237.
[13] K.L. Scrivener, A.K. Crumbie, P.L. Pratt, A study of the interfacial region between cement paste and aggregate in concrete, Mater. Res. Soc. Symp. Proc. 114 (1988) 87–88.
[14] K. Mitsui, Z. Li, D.A. Lange, S.P. Shah, Relationship between microstructure and mechanical properties of the paste–aggregate interface, ACI Mater. J. 91 (1994) 30–39.
[15] G. Giaccio, R. Zerbino, Failure mechanism of concrete-combined effects of coarse aggregates and strength level, Adv. Cem. Mater. 7 (1998) 41–48.
[16] U. Trende, O. Büyüköztürk, Size effect and influence of aggregate roughness in interface fracture of concrete composites, ACI Mater. J. 95 (1998) 331–338.
[17] D.P. Bentz, Influence of silica fume on diffusivity in cement-based materials: II. Multi-scale modeling of concrete diffusivity, Cem. Concr. Res. 30 (2000) 1121–1129.
[18] A.M. Neville, Properties of Concrete, Longman Publishers, Essex, 1997.
[19] C. Shi, P. Xie, Interface between cement paste and quartz sand in alkali-activated slag mortars, Cem. Concr. Res. 28 (1998) 887–896.
[20] A.R. Brough, A. Atkinson, Automated identification of the aggregate–paste interfacial transition zone in mortars of silica sand with Portland or alkali-activated slag cement paste, Cem. Concr. Res. 30 (2000) 849–854.
[21] A.R. Brough, A. Atkinson, Sodium silicate-based alkali-activated slag mortars: Part I. Strength, hydration and microstructure, Cem. Concr. Res. 32 (2002) 865–879.
[22] W.K.W. Lee, J.S.J. Van Deventer, The effects of inorganic salt contamination on the strength and durability of geopolymers, Colloids Surf., A 211 (2002) 115–126.
[23] W.K.W. Lee, Solid–gel interactions in geopolymers, PhD thesis, The University of Melbourne, Australia, 2003.
[24] W.K.W. Lee, J.S.J. Van Deventer, Effects of anions on the formation of aluminosilicate gel in geopolymers, Ind. Eng. Chem. Res. 41 (2002) 4550–4558.

[25] B.D. Barnes, S. Diamond, W.L. Dolch, The contact zone between Portland cement paste and glass 'aggregate' surfaces, Cem. Concr. Res. 8 (1978) 233–244.
[26] I. Jawed, J. Skalny, J.F. Young, Hydration of Portland cement, in: P. Barnes (Ed.), Structure and Performance of Cements, Applied Science, London, 1983, p. 237.
[27] S. Mindess, J.F. Young, Concrete, Prentice-Hall, New Jersey, 1981.
[28] H.N. Stein, J.M. Stevels, Influence of silica on the hydration of $3CaO{\cdot}SiO_2$, J. Appl. Chem. 14 (1964) 338–346.
[29] R.K. Iler, The Chemistry of Silica, Wiley, New York, 1979.
[30] T.B. Bergstrom, H.M. Jennings, On the formation of bonds in tricalcium silicate pastes as observed by scanning electron microscopy, J. Mater. Sci. Lett. 11 (1992) 1620–1622.
[31] P. Meredith, A.M. Donald, Pre-induction and induction hydration of tricalcium silicate: an environmental scanning electron microscopy study, J. Mater. Sci. 30 (1995) 1921–1930.
[32] J.F. Young, H.S. Tong, R.L. Berger, Compositions of solutions in contact with hydrating tricalcium silicate pastes, J. Am. Ceram. Soc. 60 (1977) 193–198.
[33] K.O. Kjellsen, O.H. Wallevik, L. Fjällberg, Microstructure and microchemistry of the paste–aggregate interfacial transition zone of high-performance concrete, Adv. Cem. Res. 10 (1998) 33–40.
[34] D. Zampini, S.P. Shah, Early age microstructure of the paste–aggregate interface and its evolution, J. Mater. Res. 13 (1998) 1888–1898.
[35] L. Jiang, The interfacial zone and bond strength between aggregates and cement pastes incorporating high volumes of fly ash, Cem. Concr. Compos. 21 (1999) 313–316.
[36] V. Yogendran, B.W. Langan, M.A. Ward, Hydration of cement and silica fume paste, Cem. Concr. Res. 21 (1991) 691–708.
[37] G. Sun, A.R. Brough, J.F. Young, ^{29}Si NMR study of the hydration of Ca_3SiO_5 and β-Ca_2SiO_4 in the presence of silica fume, J. Am. Ceram. Soc. 82 (1999) 3225–3230.
[38] Y.L. Wong, L. Lam, C.S. Poon, F.P. Zhou, Properties of fly ash-modified cement mortar–aggregate interfaces, Cem. Concr. Res. 29 (1999) 1905–1913.
[39] C.K. Yip, J.S.J. Van Deventer, Effect of granulated blast furnace slag on geopolymerisation, Proceedings of the 6th World Congress of Chemical Engineering, Melbourne, Australia, 2001, CD-ROM.
[40] H. Xu, J.S.J. Van Deventer, The geopolymerisation of alumino-silicate minerals, Int. J. Miner. Process. 59 (2000) 247–266.